Tidal turbulence in medium depth water, primarily a model study

Göran Broström, Sam Fredriksson, Nimal Sudhan Saravana Prabahar

Abstract—**Tidal energy is considered to be one important future source of renewable energy. There is presently a strong development in new technology, and there is an emerging need to e.g., describe the turbulence intensity and its characteristics in a tidal stream. In this study we consider a high-resolution Large Eddy Simulation (LES) in water with 80 m depth and a tidal stream with a maximum volume mean flow amplitude of 2 ms^{-1}. The simulation is designed to describe turbulence characteristics at a developer site outside Holyhead in the Irish Sea. We find that the turbulence intensity and e.g., its probability density function has clear time dependence, and that it is 100% stronger on the retarding tidal current as compared to the accelerating tidal current. We also find that it depends on the distance from the bottom. The turbulence is highly anisotropic with much longer length scales in the flow directions than perpendicular to flow direction. The simulation setup and results for mean flow quantities and turbulence measures are discussed in the presentation. Finally, results are compared with results from a ship mounted ADCP for mean flow characteristics and for turbulence quantities. We e.g., find that the LES model shows lower value on turbulence intensity than derived from ADCP although the reason is not identified.**

Keywords—**tidal flow, LES, turbulence, vertical structure.**

I. Introduction

TIDAL power plants operate in a harsh environment that influences maintenance costs and lifetime of equipment [2-6]. Accordingly, careful design of tidal power plants is required for successful deployment and operation. One key ingredient is knowledge of the environment where the power plants will operate. Power plants will be placed in strong tidal flows with various designs of the power plant. Design ranges from enclosed bays where turbines are put in the in- and out-flow, here the strength of the flow can to some extent be regulated. Turbines with circulating blades (the rotation axis can be both horizontal and vertical) mounted on a fundament or a floating structure is a common [7]. A novel tidal power plan designed by company Minesto uses a kite, with an attached turbine, that swings back and forth (essentially) perpendicular to the main current flow. The kite reaches velocities of 5-7 times the speed of the tidal flow and can thus use a small turbine attached to the kite.

The tide are rotationally dominated Kelvin waves and are more or less trapped to coastal areas; they have a typical scale out from the coast of say 100 km (or the barotropic Rossby radius or barotropic radius of deformation). The mean flow is thus parallel to the coast. Large-scale variation in sea surface height forces the local current while bottom friction will dampen the currents. The friction will also create turbulence that depends on the strength of the current, the bottom topography, the characteristic of the bottom, distance from bottom, phase in the tidal flow etc [8-12]. However, it is reasonable to expect that the turbulent fluctuations are say 5-20% of the mean flow but more quantitative determination requires detailed observation and modelling.

In this study we use a state-of-the art numerical model that uses the Large Eddy Simulation (LES) technique to resolve energy containing eddies enabling a thorough study of turbulence characteristics in a tidal flow [13-15]. The turbulent dissipation and mixing on small scales is parameterized using a size selective eddy viscosity concept [16]. LES type of models are frequently used for studies of boundary layer turbulence in both bottom boundary layers in atmosphere and (mainly upper) ocean dynamics [17-20]. LES model are also commonly used in wind power industry for site characterization and for studies of wind mills and impact on flow [21-24]. In this study we find, not surprisingly, that turbulence characteristics for medium depth (80 m) depend strongly on distance from bottom and phase in the tidal flow. Some theoretical concepts are outlined in section 2, where

We acknowledge funding from Swedish Energy Agency through projects 42247-1 and 42247-2. The computations were enabled by resources provided by the Swedish National Infrastructure for Computing (SNIC) at C3SE and NSC partially funded by the Swedish Research Council through grant agreements no. SNIC 2020/1-32, SNIC2019-1-42 and SNIC2018-1-42.

Göran Broström (e-mail: goran.brostrom@marine.gu.se), Sam Fredriksson (e-mail: sam.fredriksson@marine.gu.se), and Nimal Sudhan Saravana Prabahar (e-mail: nimal.sudhan.saravana.prabahar@gu.se) and are affiliated to the Department of Marine Sciences, University of Gothenburg, Box 46, SE-405 30, Gothenburg, Sweden. Sam Fredriksson is also affiliated to Swedish Meteorological and Hydrological Institute, Sven Källfelts gata 15, SE-426 71, Gothenburg, Sweden.

Digital Object Identifier: https://doi.org/10.36688/ewtec-2023-566

also the numerical model is described. The model results are shown in section 3 and discussed in section 4.

II. METHODS

A. Some basic theory

1) An idealized model for the mean flow

The mean flow situation we consider is in many ways one-dimensional, i.e., we have variations in vertical direction z while we do not have variations in mean flow in horizontal directions x, y. We consider an intermediate time scale such that horizontal turbulence fluctuations evens out, but still small as compared to the scale of the tidal wave. Observations show that the flow is swinging back and forth and that the rotational dynamics are relatively weak. For a one-dimensional flow with no gradient in the horizontal and where we neglect Coriolis force (or assume that the Coriolis force is balanced by a pressure gradients out from the coast) for the areal mean flow in x-direction, $\overline{U(z)} = \frac{1}{a}\int u dA$ ($u(x,y,z)$ is the total velocity field in the x-direction, we introduce this definition here to have a consistent formulation when discussing model results) we have

$$\frac{\partial \overline{U(z)}}{\partial t} = \frac{1}{\rho}\frac{\partial \tau}{\partial z} + f_x(t), \tag{1}$$

where τ is the vertical stress, ρ [≈1027 kgm^{-3}] is the density of sea water, and f_x is the depth independent pressure force in the x-direction (or gradient in sea surface height) driven by the tidal wave. The stress is essentially turbulent and is given by

$$\tau = -\rho\langle u'w'\rangle, \tag{2}$$

where u', w' are turbulent fluctuations in x, z directions, respectively. The boundary conditions are wind stress at the surface while there is a no-slip condition at the bottom (in practice the stress at the bottom is related to the mean flow). Here we will neglect the wind stress. By integrating (1) between the bottom ($z = -D$) to the surface (at $z = 0$ as we neglect vertical movements of the free surface) the prognostic equation for the volume mean flow $\overline{U} = \frac{1}{V}\int u dV$ can be written

$$D\frac{\partial \overline{U}}{\partial t} = DF_{acc} - \frac{\tau_b}{\rho}, \tag{3}$$

where

$$F_{acc} = \frac{1}{D}\int_{-D}^{0} f_x(t)dz, \tag{4}$$

is the imposed acceleration of the volume mean flow (i.e. it arises from remotely forced variations in the sea surface height). In this study we assume a simple tidal cycle such that forcing varies as $\cos(\omega t)$, where $\omega = 2\pi/T_{tidal}$ and the tidal period is T_{tidal} = 12 h, but other time dependence of the forcing can easily be considered as well.

2) Stress at bottom

The stress at the bottom taking velocity direction into account

$$\tau_b = \rho C_D \overline{U}|\overline{U}|, \tag{5}$$

where C_D is a drag coefficient. Using logarithmic boundary layer one can derive

$$C_D(\mathrm{z}) = \left(\frac{1}{\kappa}\ln\left(\frac{z}{z_0}\right)\right)^{-2}, \tag{6}$$

where κ=0.42 is the von Karman constant. C_D increases with distance from the bottom and with the roughness length. With z_0=0.01 m (see below), we find that $C_D(40\mathrm{m})$ ≈2.3·10^{-3}, which is the value we use in the vertically integrated model described above. The relation between friction velocity, u_*, and stress reads

$$u_* = \sqrt{\tau/\rho} \tag{7}$$

3) More on the roughness length

The LES model we consider uses the log layer as a wall function and turbulence intensity and stress at the bottom thus depend strongly on the roughness length [13, 26]. We thus need to consider this parameter in more detail. Areas with strong tidal flows often have a rather rough bottom as fine scale sediment are injected into the water and removed from the area. Various bed-forms are often generated as well [27]. For the site we consider, multi-beam echo sounding clearly show that this is the case for the Minesto development area. The survey also showed frequent (approximately 1.6/(100m)^2) large boulders with about 1-3 m characteristic size. It is not straightforward to recast this information into bottom roughness parameter. However, if we separate the bottom stress into the mean characteristic of in-between boulders (here assuming sandy bottom) and the boulders the stress towards the bottom is

$$A\tau_b = \sum \tau_{b-Boulders} + (A - A_B)\tau_{b-sand}, \tag{8}$$

where A represents the total bottom area and A_B the area covered by boulders (which is negligible compared to A). For the stress on the boulders we use

$$\tau_{b-Boulders} = \rho A_{Boulders}\frac{1}{2}C_{D-Boulders}U^2, \tag{9}$$

treating boulders as a simple sphere we use $C_{D-Boulders}$ ≈1 and $A_{Boulders}$ is the cross-section area of the blocks. By summing over all blocks available for their cross-section area and assuming sand in-between the blocks (personal communication, Minesto) with a roughness length of 0.001 m, we can use (5-9) to estimate an effective

roughness parameter for the mean area. We find approximately $z_0 \approx 0.01$ m with this approach; furthermore, it is clear that the boulders dominate the bottom stress.

B. Model description

The code used here is a Large Eddy Simulation (LES) model for the atmospheric boundary layer, and upper ocean dynamics, developed by National Centre for Atmospheric Research (NCAR), Boulder, Colorado [13, 15, 28-30]. The model describes the turbulence motions on scales larger than the grid resolution but parameterizes the Sub Grid Scales (SGS) turbulence characteristics. The SGS model uses a prognostic equation for the SGS turbulent kinetic energy [16] and uses an algebraic formulation for the turbulent length scales to close the system and describe the SGS eddy viscosity.

The implementation is based on an efficient pseudo-spectral method in the horizontal direction while using finite differences in the vertical direction. The pseudo-spectral method implies that we are restricted to periodic boundary conditions in the horizontal direction. The time stepping uses an adaptive third order Runge-Kutta scheme with an adaptive time stepping based on a prescribed CFL criteria. A centred second order finite difference scheme is used in vertical. A free slip boundary condition is applied at the surface.

The bottom roughness is set to value z_0 =0.01 m in the model. It should be noted that this represents a mean roughness over the entire area including boulders. The model assumes that the lowest grid point in the model is in a log layer and uses matching of flow variables to a Monin-Obukhov logarithmic layer [13, 16].

The model results show that the turbulence is highly anisotropic, and eddies are elongated in the flow direction. The largest eddies are of order 100-150 m in the x-direction and 15-30 m in the y-direction. The domain was chosen to encompass about 10 horizontal eddies to avoid locking the flow on specific length scales. The rather large physical domain implies that the resolution has to be restricted given the core hours available to the project. The computational domain is (1280m, 320m, 80m) in (x, y, z) directions, with (2048, 512, 128) grid points. The resolution is thus 0.625 m.

The model is forced with a simple volume force that is constant in space and varies in time; we consider this to represent an externally forced gradient in the sea level due to the tidal wave. We have not included the Coriolis force as observations clearly show a current that swings back and forth with little veering in the vertical (not shown), and our interpretation is that the Coriolis force is well-balanced by a pressure gradient out from the coast, as is expected for Kelvin waves. We have adjusted the strength of the force to give a maximum volume mean flows of 2.0 ms^{-1}.

C. ADCP observations

Acoustic Doppler Current Profiler (ADCP) measurements were taken at Holy head by Minesto AB during the testing of their tidal power generator on 30th August 2018. The ship-mounted ADCP measured data for 6.5 hours and covered both the accelerating and decelerating phase of the tidal cycle. Here, these observations are used to study the velocity profile and turbulence intensities. The ADCP used was Teledyne instruments Workhorse with a sampling frequency of 0.455 Hz, and a bin size of 4m. ADCP velocities in the earth coordinates are converted to the tidal stream coordinates, with x, y, and z as the stream, cross stream and vertical directions.

III. RESULTS

A. Mean flow

1) Volume mean flow

The simulations we consider have a cosine function in time volume force in x-direction. This implies that after 1-2 cycles we get we get a periodic solution with constant amplitude. Observations at Holyhead Deep show that the tidal currents change on a monthly scale, furthermore, currents are slightly different when moving northwards with the tidal wave direction as compared to the case when the current moves southwards against the tidal wave direction (not shown). The reason is not known and may be due to topographic differences or due to non-linear effects from the flow and changes in sea surface height. Anyway, we argue that the model describes the tidal currents well for a specific strength of the tidal current (which changes slowly on a monthly time scale) after a spin up of 1.5 tidal cycles

Fig. 1(a) shows the volume mean flow, $\bar{U}$, as a function of time. We see that the vertically integrated (idealized) model with an idealized bottom friction, (5), describes the volume mean flow very well. It should be noted that the flow is not in phase with the tidal forcing and that it becomes asymmetric in time due to the bottom friction, the peaks appears before the tidal forcing changes sign (in a friction free system, the maximum volume mean flow appears when the forcing changes sign at 27 hours, or t = 2.25 T_{tidal}). The flow also becomes asymmetric around the tidal peaks; this feature becomes more pronounced for stronger volume mean flows and stronger friction (not shown). The vertical black lines represent the time, t_{peak}, when the flow is at the maximum mean flow (thick line) and the times, $t_{80\%}$, where the volume mean flow is 80% of the maximum volume mean flow (thinner lines on each side of the peak). Fig. 1(b) shows the predictions of the maximum currents on the second tidal peak from LES model and the idealized model Eqs (3, 5, 6). The good agreement between the idealized model and the LES model highlights the possibility to use the idealized model for evaluating, and adjusting parameters for, the more complex LES model. As an example, we can use the

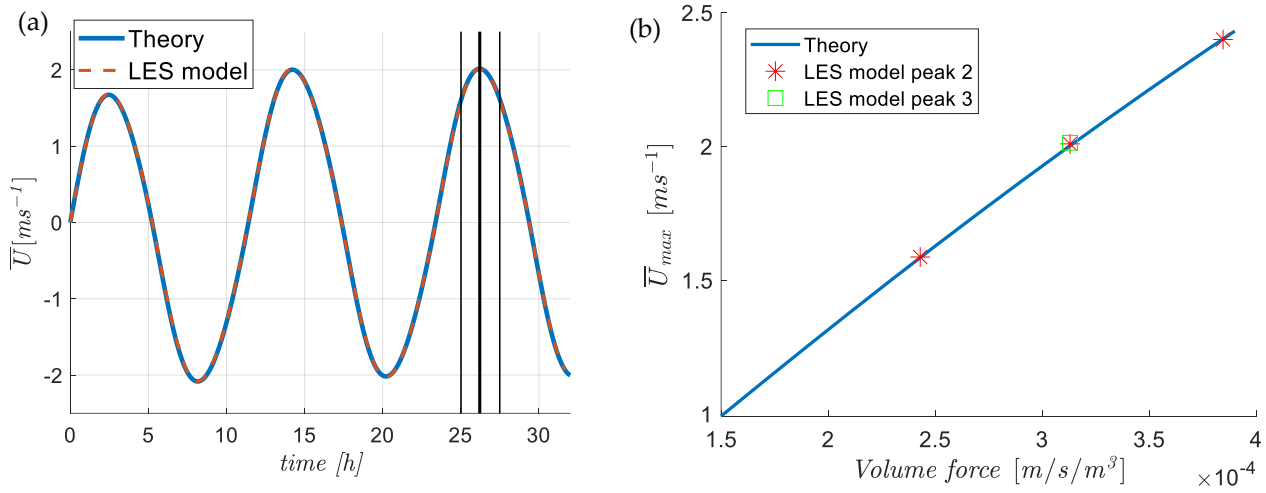

Fig. 1(a). Comparison of mean current for the simple and LES "tidal" model having the same volume force. Drag coefficient is about $2.3{\cdot}10^{-3}$, i.e., it is calculated according to (10) using z_0 =0.01 m and z=40 m from bottom. The times where the flow is at the third maximum, t_{peak}, is shown with a thick vertical line and the times where the volume mean flow is at 80% of the maximum flow, $t_{80\%}$, are shown with thin vertical lines. Fig. 1(b). shows the time evolution for the 2 ms^{-1} volume mean flow case (maximum volume force $3.13{\cdot}10^{-4}$ $ms^{-1}m^{-3}$). Fig. 1(b) shows the maximum volume mean velocities at the second maximum (one point showing the value at the third peak for the standard run, which was longer than the non-standard runs, as a function of the reference volume force.

idealized model to adjust the strength of the volume force to provide a pre-decided volume mean flow.

2) Areal mean flow profiles

Here we consider the areal mean of the u-velocity, $(\overline{U(z)})$, at the time of the maximum volume mean flow, shown as a thick black line in Fig. 2. It should be noted that the horizontal mean of the v- and w-velocities are zero. Observation from an ADCP located a few kms toward the south. And at a slightly deeper location, is shown as gray lines. The bottom characteristics at the site of the ADCP is not entirely known. Although this uncertainty, the model reproduces the vertical structure of the areal mean flow well.

3) Bottom friction velocity as function of time

The mean friction velocity at the bottom, u_*, is a key parameter/quantity for evaluating the turbulence level in the flow, and it is shown in Fig. 3. The friction velocity in the idealized model is calculated according to (5, 6), and is thus linearly related to the strength of the flow. In the LES model it evolves with the mean flow in the vicinity of the bottom and the modelled turbulence levels. We see that the idealized model captures the friction velocity well, and thus the bottom stress, again showing that key features of the flow can be captured with the idealized model.

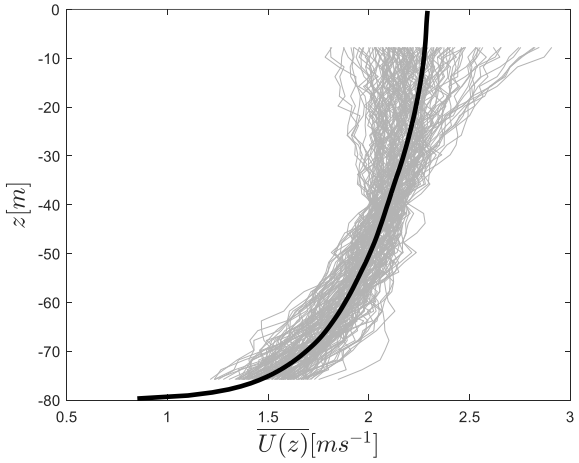

Fig. 2. Areal mean flow at the tidal peak, black line is areal mean of the model flow in the direction of the tidal flow and gray lines are ADCP observations at different times. The observations are from a relatively nearby site that is 100 m deep as compared to model simulation that has depth 80 m. We have extracted the observed velocities that have value of 2.1±0.1 ms^{-1} at 40 m from the bottom (i.e. 2.1 ms^{-1} represent the model areal mean velocity 40 m from bottom).

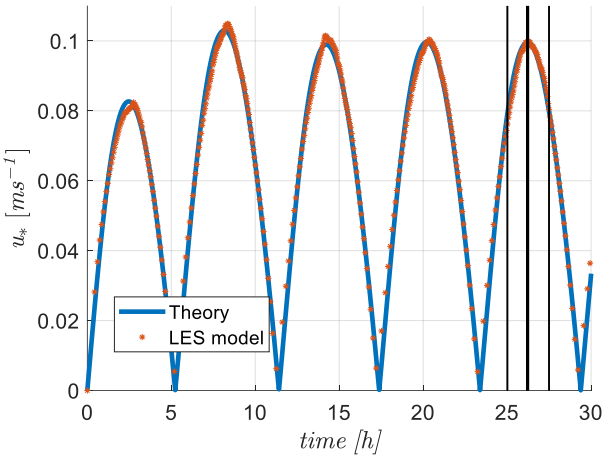

Fig. 3. The bottom friction velocity as a function of time for the simple model and the LES model for the standard case. The time for the t_{peak} and $t_{80\%}$ are shown as vertical lines. The output from the LES model is once every 1000 time steps.

B. Turbulence characteristics

1) Instantaneous fields

It is useful to first display how the instantaneous velocity fields look like before a more detailed analysis is considered. Accordingly, snapshots of the velocity fields are shown in Fig. 4. We see that the velocity fluctuations are larger in the x-direction (mean flow direction) than in the other two directions. We also see that the vertical turbulent fluctuations (i.e., the w-field) has small spots of intensive positive flow ejecting boundary properties into the mean flow. The figures show that the structures are largest in the x-direction, followed by the y-direction while they seem to be smallest in the vertical direction (as judged from the small-scale structures in the w-field). We conclude that the model domain is large enough to allow for several eddies in the domain, and there is no locking of turbulent eddies to the domain size.

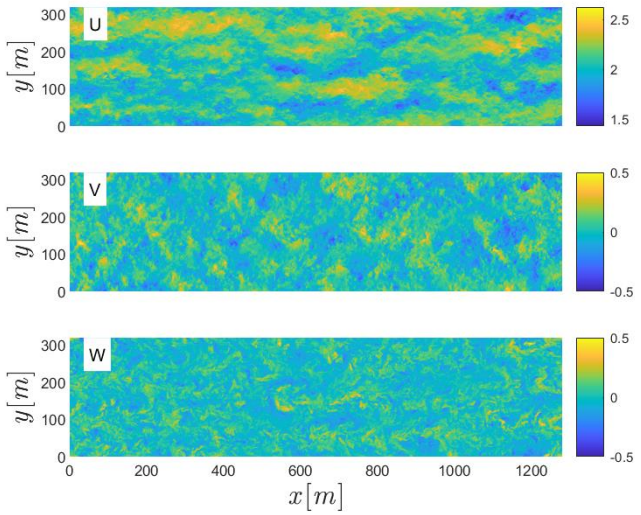

Fig. 4. Instantaneous model velocities at the maximum of the third tidal peak. The sections are at z=40 m depth. Color scales are in ms^{-1}.

2) Vertical variation of turbulence quantities

The strength of the turbulence field and how it influences structures are key questions for designing equipment to be optimized for flow conditions. The turbulence intensity, I, which is the strength of the velocity fluctuations scaled with some mean flow quantity, is frequently used to characterize the turbulence. However, there are several choices for which mean flow to use e.g., the local time average, the areal mean flow, the volume mean flow or maximum values of the flow, and the choice will change the actual value of I for the same level of turbulence. For modelling studies all these different quantities are readily available. For pointwise observational flows the local mean flow over some time is most readily available, although the maximum velocity can also be found if the measurement time series is long enough.

We define the turbulence intensity as [9, 10]

$$I_x = \frac{\sigma_x}{\overline{U}}, \tag{10}$$

where

$$\sigma_x^2 = Var(x), \tag{11}$$

is for arbitrary velocity component, here Var is the variance of the arbitrary variable x and $\overline{U}$ is some mean velocity. Furthermore

$$\sigma_q^2 = \sigma_u^2 + \sigma_v^2 + \sigma_w^2, \tag{12}$$

where q is the total velocity variation $q^2 = u'^2+v'^2+w'^2$ (which relates to the turbulent kinetic energy, k, as $k = q^2/2$).

The turbulence intensity field $\sigma(q)$ using areal mean flow $\overline{U(z)}$ as the mean scaling velocity (this correspond to the case with observations taken at discrete depths), is shown in Fig. 5 that shows the vertical structure of scaled turbulence quantities for the same volume mean flow, but before and after the tidal peak. The turbulence intensity for this specific case (having volume mean flow 1.6 ms^{-1}) increase by about 100% from before the peak to after the peak. The figure also shows that turbulence intensity decrease quickly from the bottom into the interior. It is also seen that the variance is anisotropic, and that the turbulence intensity is strongest for the u-velocity (in the direction of the flow) followed by v-velocity and the turbulence intensity is weakest in the vertical velocity.

The relation between the standard deviations for the velocity components reflects the anisotropy of the turbulence field (see Fig. 5(b)). Earlier studies point towards that for 5 m from the bottom [6, 10] σ_u: σ_v: σ_w = 1:0.75:0.56. Studies from channel flow [11] σ_u: σ_v: σ_w = 1:0.71:0.55 and atmosphere [31] σ_u: σ_v: σ_w = 1:0.68:0.45 are in the same ballpark. This fits well with values a few meters from the bottom. However, we also see that these quantities depend on the distance form bottom, we also see a clear time dependence, e.g., when comparing quantities at same volume mean flow but before and after the peak. As expected, the anisotropy is stronger after the peak flow than before the peak flow.

3) Turbulent kinetic energy

The turbulent kinetic energy (TKE), or q, is key variable in understanding turbulence. The value of q normalized by the friction velocity is displayed in Fig. 6. At the bottom it increases with the tide, the peak in q/u_* is slightly after the maximum tide (thick black line). We also see that the turbulence moves up from the bottom as time progresses reaching the surface $0.2\,T_{tidal}$ after the turning tide (the tide turns at about t = $1.95\,T_{tidal}$). The peak in q/u_* thus occurs later when moving towards the surface. The decline in q/u_* with time after the peak flow is somewhat slower than the rise before the peak flow.

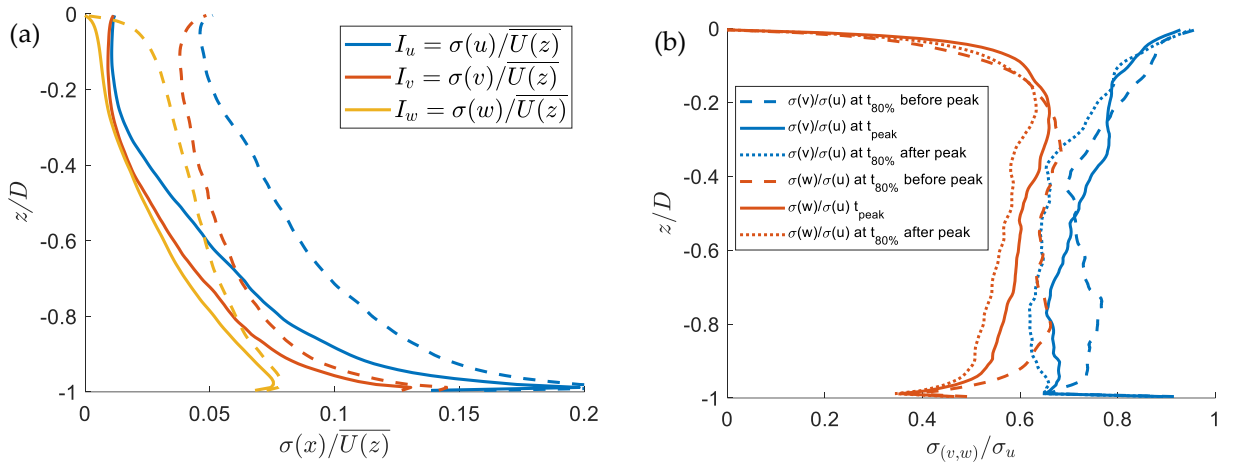

Fig. 5(a). The turbulent intensities for different velocity components normalized by the areal mean flow. Fig. 5(b). Ratios of turbulence intensities, or anisotropy. The curves represent the same volume mean flow of the tidal current but before (solid lines) and after the peak (dashed lines). The times correspond to the thin black lines in Fig. 1(a).

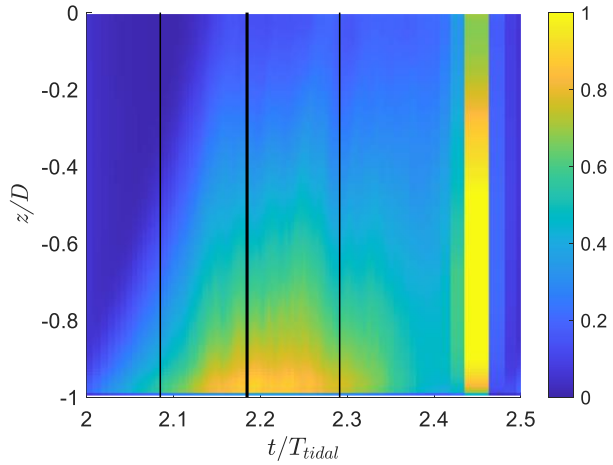

Fig. 6. Contour plot of total velocity fluctuations normalized by the friction velocity, i.e., q/u_*. High values at turning tide is because u_* becomes small. Thick black line is at the peak in mean flow, t_{peak}, and thin black lines represents $t_{80\%}$ before and after the peak.

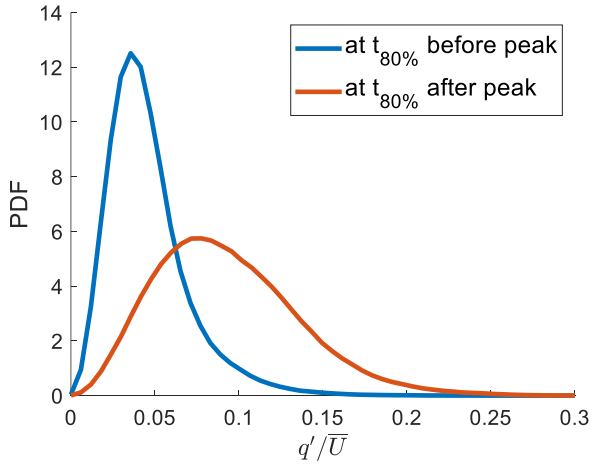

Fig. 7. The normalized probability density function of the velocity scale q at z=40 m at times when the flow is 80% of maximum before peak, at peak, and 80% of maximum after the peak.

C. *Probability density functions*

As stated, the magnitude of the turbulent fluctuations are important for designing equipment that will operate in a turbulent tidal flow [33]. If we plot the normalized probability density distribution for the velocity scale, q we notice that the velocity distribution is wider after the tidal peak than before the tidal peak (Fig. 7). It is thus likely that turbulence is a greater problem in the late stage of the tidal cycle than in the initial part. These kinds of distributions are important for various life cycle analyses and reliability engineering [33, 34].

For survival of equipment, it is likely that it is the most energetic part of the distribution that the construction needs to be designed for. For instance, the mean of q for the highest 95% percentile are 0.11 and 0.2 $\overline{U}$ for the two cases.

D. *ADCP Observations*

1) *Mean flow velocity*

From the ADCP observations, the tidal cycle has a time period of 6 hours, which is comparable to the model; however, the peak tidal velocity is less than 2 ms^{-1}, which is lower compared to the model (see Fig. 8). Time averaged stream velocity profiles at 70% of the peak flow ($t_{70\%}$) is plotted in Fig. 8. $t_{70\%}$ is used here instead of the $t_{80\%}$ because at $t_{80\%}$ before the peak, the tidal power generator was running, and its wake significantly affects the results. Time averaging was done for 1000 seconds. The velocity profiles exhibit different features before and after the peak, with higher velocities close to the bottom after the peak. In depths less than 70 m, the velocities are higher before the peak. This is expected in the velocity profiles during the accelerating and decelerating phases [35]. At 40 m depth, where tidal generators might operate, the velocity is slightly lower in the decelerating phase than in the accelerating phase.

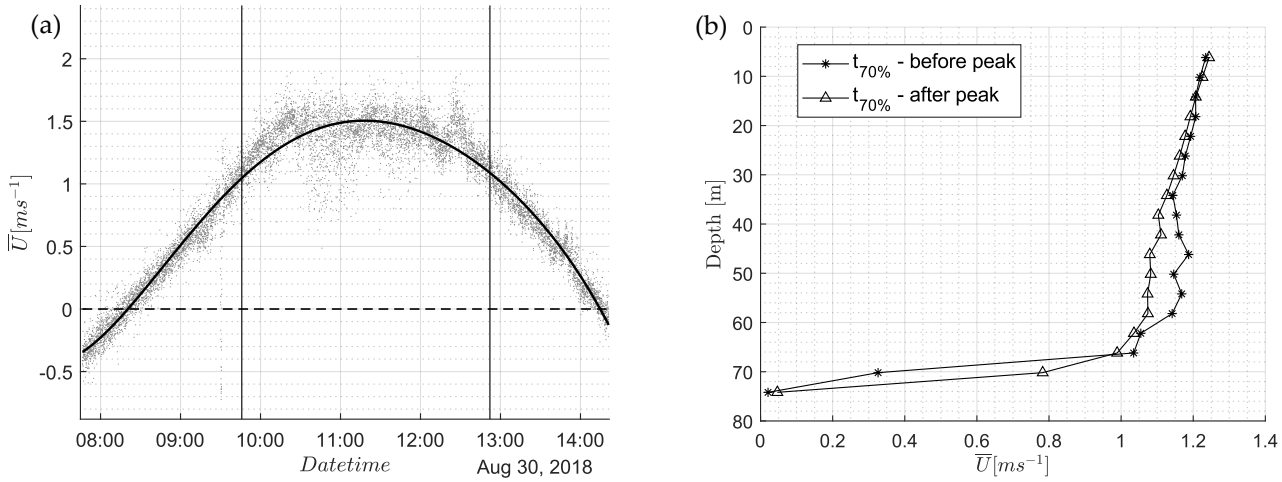

Fig. 8(a). Vertically integrated flow velocity for the ADCP observations, dots are the observations, and the curve is a 5th order polynomial fit. Vertical line indicate the locations $t_{70\%}$ where flow is 70% of the peak. Fig. 8(b). Time-averaged profile of the stream velocity for 70% of the peak tidal flow before and after the peak. $t_{70\%}$ is used instead of $t_{80\%}$ because at $t_{80\%}$ before the peak, the tidal power generator was running, and it significantly affects the results

2) *Turbulence Intensity*

Turbulence intensity from the observations is calculated using (10) and (11). The observations have a significant amount of noise and errors [36-38]. Hence as an effort to reduce noise, outliers beyond 3 standard deviations are removed during the calculation of variance [39]. Fig. 9 shows the turbulence intensity for the different velocity components. It is seen that the turbulence intensity increased significantly towards the rough bottom. The stream component is the highest and all the components are higher after the peak than before the peak. This trend is comparable to the model results in Fig. 5. However, the turbulence intensity in the observations is higher than the model; this could be due to instrument noise and other disturbances. It might also infer that the turbulence is higher in real conditions than in the model, e.g., indicating a too low value of z_0 is used.. The turbulence intensity of the stream velocity close to the surface is higher before the peak than after the peak. This trend is not seen in the model results and can be due to e.g., wind that is absent in model..

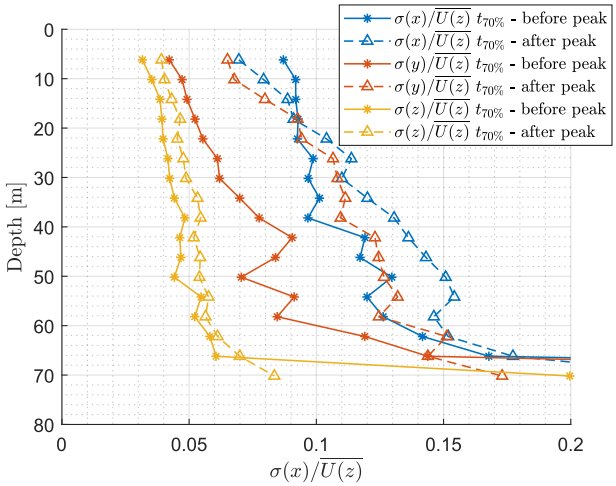

Fig. 9. The turbulent intensities for different velocity components normalized by the mean flow from the ADPC observations at 70% of the peak flow before and after the peak. To remove signal noise valued outside 3 standard deviations are removed while calculating variance

IV. Discussion and Conclusion

Tidal power has the potential to become an important component of renewable energy and the devices needed to extract power in a tidal flow are continuously developing. The tidal environment is, however, harsh with strong flows, strong turbulence and possible variable wave action and need therefore to be well characterized in order to facilitate this development. There will be environmental impacts when extracting tidal power, these will be both local, and if they become abundant also remote environmental impacts. The local impact most likely depends on the impact on the local flow and associated changes in turbulence.

In this study, we use a state-of-the-art LES model developed for boundary layer dynamics in the atmosphere and the ocean. We force the model with a cyclic in time volume force that creates a tidal-like flow. We consider a case study for the tidal flow outside the Wales coast, or outside Holyhead to be more specific. This is the development site for the company Minesto that develops a "kite" that will flow through the tidal current. The device operates in relatively deep water and the equipment undergoes testing in 80 m deep water, which is also the depth of the tidal current in this model study.

We find that the turbulence intensity has a strong time dependence and that it evolves over the tidal cycle. Accordingly, the same volume mean flow can have quite different turbulence characteristics for the same volume

mean flow. The flow profile in general shows resemblance to a log layer even though we do not have constant flux layer as is the basis for the "log layer" theory. This resemblance is for instance manifested by that the idealized integrated model gives very accurate predictions on mean flow and the friction velocity (and thus bottom stress).

If we look at the site for this study the bottom friction, or roughness length, is dominated by well-separated large blocks. Close to the bottom we expect that the turbulence is higher behind these blocks than in surrounding areas with smooth bottom. How far away from bottom, and the blocks, this anisotropy will remain is unknown and may impact on the turbulence levels at separate power plants in a power plant park. This is beyond the aim of the present study but may be an important aspect for power park development.

ADCP observations and model correlated well with model although some differences. The increase in turbulence intensity after the peak was seen in the observations, which was correctly predicted by the model. However, the overall magnitude of the turbulence intensity was higher in the observations and the reasons behind this need to be investigated. Also, turbulence computation from ADCP observations does not cover all the length and time scales.

ACKNOWLEDGEMENT

We acknowledge funding from Swedish Energy Agency through projects 42247-1 and 42247-2. The computations were enabled by resources provided by the Swedish National Infrastructure for Computing (SNIC) at C3SE and NSC partially funded by the Swedish Research Council through grant agreements no. SNIC 2020/1-32, SNIC2019-1-42 and SNIC2018-1-42.

REFERENCES

[1] W. Munk, C. Wunsch, Abyssal recipes II: Energetics of tidal and wind mixing, Deep-sea research. Part I, Oceanographic research papers, 45 (1998) 1977-2010.

[2] U. Ahmed, D. Apsley, I. Afgan, T. Stallard, P. Stansby, Fluctuating loads on a tidal turbine due to velocity shear and turbulence: comparison of CFD with field data, Renewable Energy, 112 (2017) 235-246.

[3] T. Blackmore, L.E. Myers, A.S. Bahaj, Effects of turbulence on tidal turbines: implications to performance, blade loads, and condition monitoring, International Journal of Marine Energy, 14 (2016) 1-26.

[4] M.J. Churchfield, Y. Li, P.J. Moriarty, A large-eddy simulation study of wake propagation and power production in an array of tidal-current turbines, Philosophical Transactions of the Royal Society A: Mathematical, Physical and Engineering Sciences, 371 (2013) 20120421.

[5] A. Mason-Jones, D. O'doherty, C. Morris, T. O'doherty, Influence of a velocity profile & support structure on tidal stream turbine performance, Renewable Energy, 52 (2013) 23-30.

[6] I. Milne, A. Day, R. Sharma, R. Flay, The characterisation of the hydrodynamic loads on tidal turbines due to turbulence, Renewable and Sustainable Energy Reviews, 56 (2016) 851-864.

[7] D. Magagna, R. Monfardini, A. Uihlein, JRC ocean energy status report 2016 edition, Publications Office of the European Union: Luxembourg, (2016).

[8] M. Lewis, S. Neill, P. Robins, M. Hashemi, S. Ward, Characteristics of the velocity profile at tidal-stream energy sites, Renewable Energy, (2017).

[9] K. McCaffrey, B. Fox-Kemper, P.E. Hamlington, J. Thomson, Characterization of turbulence anisotropy, coherence, and intermittency at a prospective tidal energy site: Observational data analysis, Renewable Energy, 76 (2015) 441-453.

[10] I.A. Milne, R.N. Sharma, R.G. Flay, S. Bickerton, Characteristics of the turbulence in the flow at a tidal stream power site, Phil. Trans. R. Soc. A, 371 (2013) 20120196.

[11] I. Nezu, H. Nakagawa, G.H. Jirka, Turbulence in open-channel flows, Journal of Hydraulic Engineering, 120 (1994) 1235-1237.

[12] M.T. Stacey, S.G. Monismith, J.R. Burau, Measurements of Reynolds stress profiles in unstratified tidal flow, Journal of Geophysical Research: Oceans, 104 (1999) 10933-10949.

[13] C.L. Lin, C.H. Moeng, P.P. Sullivan, J.C. McWilliams, The effect of surface roughness on flow structures in a neutrally stratified planetary boundary layer flow, Phys Fluids, 9 (1997) 3235-3249.

[14] P.P. Sullivan, J.C. McWilliams, C.H. Moeng, Structure of the atmospheric wave induced boundary layer, 12th Symposium on Boundary Layers and Turbulence, (1997) 304-305.

[15] P.P. Sullivan, C.H. Moeng, J.C. Mcwilliams, Large-eddy simulation of surface layer flows in the atmospheric and oceanic planetary boundary layers using grid nesting, 11th Symposium on Boundary Layers and Turbulence, (1995) 357-360.

[16] P.P. Sullivan, J.C. Mcwilliams, C.H. Moeng, A Subgrid-Scale Model for Large-Eddy Simulation of Planetary Boundary-Layer Flows, Bound-Lay Meteorol, 71 (1994) 247-276.

[17] A. Brereton, A.E. Tejada-Martínez, M.R. Palmer, J.A. Polton, The perturbation method-A novel large-eddy simulation technique to model realistic turbulence: Application to tidal flow, Ocean Modelling, 135 (2019) 31-39.

[18] S.E. Belcher, A.L. Grant, K.E. Hanley, B. Fox-Kemper, L. Van Roekel, P.P. Sullivan, W.G. Large, A. Brown, A. Hines, D. Calvert, A global perspective on Langmuir turbulence in the ocean surface boundary layer, Geophysical Research Letters, 39 (2012).

[19] T. Kukulka, A.J. Plueddemann, J.H. Trowbridge, P.P. Sullivan, Significance of Langmuir circulation in upper ocean mixing: Comparison of observations and simulations, Geophysical Research Letters, 36 (2009).

[20] J.C. McWilliams, P.P. Sullivan, Vertical mixing by Langmuir circulations, Spill Sci Technol B, 6 (2000) 225-237.

[21] R.J. Barthelmie, L. Jensen, Evaluation of wind farm efficiency and wind turbine wakes at the Nysted offshore wind farm, Wind Energy, 13 (2010) 573-586.

[22] R.J. Barthelmie, S.C. Pryor, S.T. Frandsen, K.S. Hansen, J. Schepers, K. Rados, W. Schlez, A. Neubert, L. Jensen, S. Neckelmann, Quantifying the impact of wind turbine wakes on power output at offshore wind farms, Journal of Atmospheric and Oceanic Technology, 27 (2010) 1302-1317.

[23] J.N. Sorensen, W.Z. Shen, Numerical modeling of wind turbine wakes, J. Fluids Eng., 124 (2002) 393-399.

[24] Y.-T. Wu, F. Porté-Agel, Modeling turbine wakes and power losses within a wind farm using LES: An application to the Horns Rev offshore wind farm, Renewable Energy, 75 (2015) 945-955.

[25] W. Large, S. Pond, Open ocean momentum flux measurements in moderate to strong winds, Journal of physical oceanography, 11 (1981) 324-336.

[26] R. Vasaturo, I. Kalkman, B. Blocken, P. Van Wesemael, Large eddy simulation of the neutral atmospheric boundary layer: performance evaluation of three inflow methods for terrains

with different roughness, Journal of Wind Engineering and Industrial Aerodynamics, 173 (2018) 241-261.
[27] S.J. Hulscher, H.E. de Swart, H.J. de Vriend, The generation of offshore tidal sand banks and sand waves, Continental Shelf Research, 13 (1993) 1183-1204.
[28] C.L. Lin, C.H. Moeng, P.P. Sullivan, J.C. Mcwilliams, Coherent structures and dynamics in shear-driven planetary boundary layer flows, 11th Symposium on Boundary Layers and Turbulence, (1995) 287-290.
[29] J.C. McWilliams, E. Huckle, J.H. Liang, P.P. Sullivan, The Wavy Ekman Layer: Langmuir Circulations, Breaking Waves, and Reynolds Stress, Journal of Physical Oceanography, 42 (2012) 1793-1816.
[30] J.C. McWilliams, P.P. Sullivan, C.H. Moeng, Langmuir turbulence in the ocean, Journal of Fluid Mechanics, 334 (1997) 1-30.
[31] N.J. Cook, Designers guide to wind loading of building structures. Part 1, (1986).
[32] T.M. Dillon, Vertical overturns: A comparison of Thorpe and Ozmidov length scales, Journal of Geophysical Research: Oceans, 87 (1982) 9601-9613.
[33] Y. Bai, Marine structural design, Elsevier, 2003.
[34] X. Song, S. Wang, Z. Hu, H. Li, A hybrid Rayleigh and Weibull distribution model for the short-term motion response prediction of moored floating structures, Ocean Engineering, 182 (2019) 126-136.
[35] J. Z. Shi, "Tidal resuspension and transport processes of fine sediment within the river plume in the partially-mixed Changjiang River Estuary, China: A personal perspective," *Geomorphology*, vol. 121, pp. 133–151, Sep. 2010.
[36] D. Mueller, J. Abad, C. García, J. Gartner, M. García, and K. Oberg, "Errors in Acoustic Doppler Profiler Velocity Measurements Caused by Flow Disturbance," *Journal of Hydraulic Engineering-asce - J HYDRAUL ENG-ASCE*, vol. 133, Dec. 2007.
[37] M. Thiébaut *et al.*, "Assessing the turbulent kinetic energy budget in an energetic tidal flow from measurements of coupled ADCPs," *Philosophical Transactions of the Royal Society A: Mathematical, Physical and Engineering Sciences*, vol. 378, no. 2178, p. 20190496, Jul. 2020.
[38] V. Durgesh, J. Thomson, M. C. Richmond, and B. L. Polagye, "Noise correction of turbulent spectra obtained from acoustic doppler velocimeters," *Flow Measurement and Instrumentation*, vol. 37, pp. 29–41, 2014.
[39] E. A. Nystrom, C. R. Rehmann, and K. A. Oberg, "Evaluation of Mean Velocity and Turbulence Measurements with ADCPs," *Journal of Hydraulic Engineering*, vol. 133, no. 12, pp. 1310–1318, Dec. 2007.